PCCP

Accepted Manuscript

ROYAL SOCIETY OF CHEMISTRY

www.rsc.org/pccp

PCCP

ARTICLE

Study of thermal conductivity of ice clusters after impact deposition on the silica surfaces using the ReaxFF reactive force field

Received 24th September 2015,
Accepted 00th January 20xx

DOI: 10.1039/x0xx00000x

www.rsc.org/

A.Rahnamoun[a] and A.C.T. van Duin[b]

During aircraft or spacecraft missions, ice accumulates on different parts of their surface elements. An important parameter affecting the ability to remove this ice from the surface is the heat transfer characteristics of the accumulated ice. The ice heat transfer is related to the process of ice formation and its density and internal structure. In this study we investigate the effects of ice and silica structure and the ice cluster attachment mechanism to the silica surface on the thermal conductivity (TC) of the attached ice cluster using the ReaxFF reactive force field. The purpose of this study is to investigate the thermal transport in amorphous and crystalline ice after high-velocity deposition on the silica surfaces. A dual thermostat method has been applied for the calculation of TC values. The validity of this method has been verified by comparing the calculated values of TC for crystal and amorphous ice with available experimental values. Our calculations show that the TC value for both crystal and amorphous ice drop after deposition on the silica surfaces. This decrease in the TC is more significant for the ice deposition on suboxide silica surfaces. Furthermore, crystal ice shows higher TC values than amorphous ice after accumulation. However, when crystal ice impacts on the silica surface at 1 km/s impact speed, the crystalline shape of the ice cluster is lost to a considerable level and the TC values obtained for the ice clusters in such cases are closer to amorphous ice TC values. We observed a decrease in the TC values when ionic species are added inside the ice clusters.

Introduction

For aircraft and spacecraft, ice is a threat both during flight and during take-off. Especially for aircraft, the ice accretion can decrease the lift and cause the pilot to lose control. When water droplets, which can be supercooled to -40^{0}C, impact on the cold aircraft surface, they can freeze and accumulate[1]. Ice is a source of debris from the external fuel tank of the spacecrafts that can be released during launch and has the potential to cause damage to the spacecraft surface elements.

The thermophysical properties of ice on the surface of the spacecrafts play a key role in the physics of heat conduction. There have been significant amounts of studies on thermophysical properties of materials. These studies have been conducted on materials with different complexities and different calculations methods have been applied in TC calculations[2-29].

The dominant contributors to the concept of thermal conductivity (TC) in water and ice clusters are phonons. Therefore, several methods have been developed to capture the phonon effect in predicting TC [30-33].Various different approaches have been applied in the calculation of TC of materials. One of the most straightforward methods applied in determination of TC is direct method[34, 35].In the direct method, the TC is calculated as the ratio of an imposed heat flux to the resulting temperature gradient. The heat flux is imposed by adding kinetic energy from hot side and withdrawing kinetic energy from cold side of the system. Another method for computation of TC is the Green–Kubo method[36]. In this method, the TC is calculated in terms of the integral of correlation functions. This method uses the fluctuations of the heat current in a homogeneous equilibrium system to calculate the TC applying linear response theory. Other methods include the thermal diffusion method[37], Evans homogeneous field method[38] and Boltzmann transport equation[39].

At the Nano-scale, molecular structure of the materials and surfaces, and the interactions between them at the atomistic length scales play a key role in the heat transfer performance. Therefore, the molecular dynamics (MD) method emerges as a valuable method for investigation of the heat transfer in such scales. One of the objectives of this study is to use MD simulations to identify the relationship between the ice structure at the silica interface and its thermal transport properties. Because MD simulation provides the ability to

[a] Department of Mechanical and Nuclear Engineering, The Pennsylvania State University, 234 Research East, University Park, Pennsylvania 16802, USA
[b] Department of Mechanical and Nuclear Engineering, The Pennsylvania State University, 240 Research East, University Park, Pennsylvania 16802, USA

obtain the detailed information on atomic level and the associated dynamics of the structure, it is used for the atomic level evaluation of the thermal transport characteristics. The force field used for these simulations has been already developed for silica-ice interface[40] and can successfully describe water-dissociation and proton-transfer events at this interface, which can substantially affect the water/silica contact and affiliated thermal transfer.

Using ReaxFF reactive force field method, equilibrium and non-equilibrium molecular dynamics (EMD and NEMD) can be used to determine the thermal conductivity of materials, since these are computationally inexpensive and combine well with the relatively expensive ReaxFF force engine. In EMD method, an equilibrated system is used and the TC value is calculated with application of statistical averaging .In NEMD method, the TC value is calculated using cooling/heating rates monitoring. The EMD and NEMD approaches are reliable alternatives to the traditional Green-Kubo method[41].

The ReaxFF, Reactive Force Field Method

ReaxFF reactive force field molecular dynamics program has been used for performing the simulations in this study. ReaxFF can provide the computational requirements to perform molecular dynamics simulations on systems which are sufficiently large to describe the characteristics of the materials. The ReaxFF reactive molecular dynamics program was developed based on computational chemical methods to bridge the gap between quantum chemical (QC) and empirical force field (EFF).

This program can provide the computational requirements to perform molecular dynamics simulations on systems which are sufficiently large for TC-evaluation, as demonstrated previously for zinc-oxide/water interface systems[42].

ReaxFF is a general bond-order-dependent force field that provides reasonable descriptions of bond breaking and bond formation[43-51]. The main difference between traditional non-reactive force fields and ReaxFF is that in ReaxFF the connectivity is determined by bond orders calculated from interatomic distances that are updated every MD simulation step. This allows for bonds to break and form during the simulation. In order to account for nonbonded interactions such as van der Waals and Coulomb interactions for a system with changing connectivity, these interactions are calculated between every pair of atoms, irrespective of connectivity, and any excessive close-range nonbonded interactions are avoided by inclusion of a shielding term. In addition, ReaxFF accounts for polarization effects by using a geometry-dependent charge calculation scheme. In ReaxFF, valence and torsion angle energies are functions of bond order so that their energy contributions go to zero smoothly upon bond dissociation.

ReaxFF force fields are parameterized against an extensive training set consisting of bond lengths, atomic charges, valence and torsion angle energies, heats of formation and reaction energies.

Using ReaxFF, we can describe the full chemistry of many reactions. The currently available ReaxFF parameter sets can capture the chemistry of the reactions of a series of metal oxides including CuO, ZnO, SiO_2 reactions with water[40, 52, 53]and also protein and DNA descriptions[54].

In this article, we have used ReaxFF force field including silica-water parameters[40] to study the TC values of crystal and amorphous ice clusters after deposition on suboxide and fully oxidized silica surfaces.

Simulation model and method

Ice cluster impact simulations

In this research, TC values of amorphous and crystal ice clusters after deposition on fully oxidized and suboxide silica surfaces at different impact velocities are evaluated. This study can be extended to the study of ice clusters deposited on other materials such as aluminum or polymer composites. In these simulations, the ice clusters deposit on the silica surfaces after impacting the silica surfaces with impact velocities of 0, 0.5 and 1 km/s. These ice cluster impacts can happen at lower velocities during aircraft missions or even higher velocities during collisions at spacecraft surfaces. However, in this study we have focused on this range of impact velocities. The changes in impacting ice clusters thermal conductivities at this impact velocity range can pave the path to predicting the trend of changes in the thermal conductivity of ice clusters at other impact velocities.

Two different amorphous silica structures are used in these simulations. These silica structures are fully oxidized silica and suboxide silica obtained by combining SiO_2 and $SiO_{1.5}$ building molecules for fully oxidized and suboxide silica respectively. Because spacecrafts are traveling in abrasive environment, there is possibility of creating suboxide silica surfaces during the missions. Therefore, we have considered both fully oxidized and suboxide silica in these studies. The characteristics of these silica structures are mentioned in Table 1. The procedure for preparing the suboxide silica structure is shown in Figure 1. Initially, the Si_8O_{20} building blocks are put in a periodic box at low density. After this initial step, the system is compressed to reach to the high density of 2.6 g/cm^3. After this stage the surface of the silica structure is opened and the annealing process between 150K to 700K is performed. At the end of this surface opening and annealing process, the density of the silica structure which is ready for the ice deposition on top of it is 2.18 g/cm^3. The same procedure is applied for preparing the fully oxidized silica structure. The RDF graphs of the fully oxidized silica at 150K are shown in Figure 2. These graphs demonstrate good correspondence with realistic SiO_2 amorphous silica[55].

Table1. Characteristics of fully oxidized and suboxide amorphous silica structures

Amorphous silica type	Molecular formula	Total number of atoms	Molar mass (g/mole)
Fully oxidized	$Si_{870}O_{1740}$	2610	52250.46
Suboxide	$Si_{1040}O_{1560}$	2600	54140.84

Fig1. Preparation of the amorphous silica structures

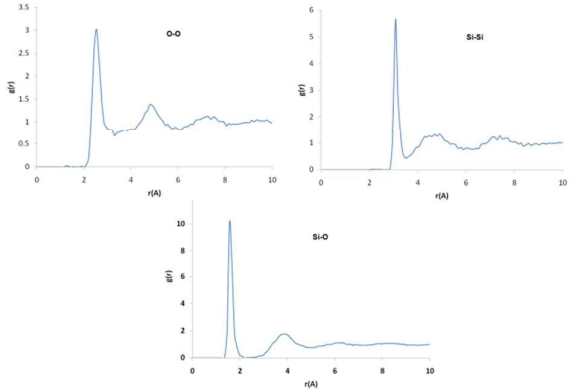

Fig2. RDFs in SiO_2 silica shown for Oxygen-Oxygen O–O, Silicon-Silicon Si–Si, and Silicon-Oxygen Si–O

The amorphous ice cluster contains 500 water molecules and the crystal ice cluster contains 512 water molecules. These ice clusters are prepared at the initial temperature of 150 K[56, 57].

The amorphous ice structure was prepared by filling a box of size 27.39×27.06×27.65 $Å^3$ with 500 water molecules. This resulted in a density of 0.98 g/cm3. The system was then equilibrated using an *NVT* ensemble at 150K.

The initial configurations of these ice clusters before the stage of shooting them towards the silica surfaces are shown in Figure 3. In order to prevent pre-collision interactions between the ice cluster and silica surface, the ice clusters are put in an initial position so that the bottom of the ice clusters are at a distance about 20Angstrom from the surface of the silica. The total system is equilibrated at 150K using NVT simulation. This temperature is in the range of the temperatures observed during operations at high altitudes from the earth surface.

In order to start the collision procedure in each simulation, a velocity normal to the surface is given to the ice cluster to obtain impact velocities of 500 m/s and 1 km/s.

In these simulations, 0.1 femto seconds (fs) time step is chosen. The molecular dynamics simulations are NVE simulations, indicating conservation of energy. The total time of the each collision simulation is 30 pico seconds (ps). During the impacts, good conservation of energy with a fluctuation of around 7kcal/mol has been observed. These fluctuations take place around the average total energy of the system with a value around -400000 kcal/mol.

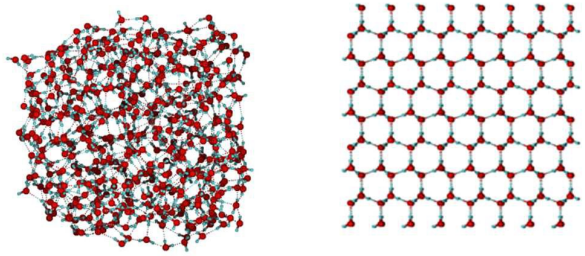

Fig3. Configuration of the amorphous and crystal ice clusters including 500 and 512 water molecules respectively and equilibrated at the initial temperature of 150K

Figure 4 shows several snapshots of the crystal ice impacting on the fully oxidized silica surface at two different impact velocities 500m/s and 1 km/s. The loss of crystallinity is more significant in the 1 km/s impact compared to 500m/s impact. This causes a decrease in the TC values of ice cluster which will be discussed later.

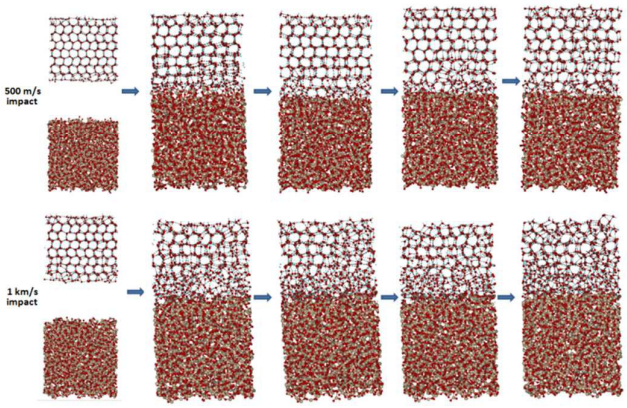

Fig4. Snapshots of crystalice cluster- silica impact simulation. The crystal ice impacts on the fully oxidized silica surface at two different impact velocities - 500m/s and 1 km/s

The dual thermostat method

In the dual thermostat method, two thermostats are applied to different ends of the system. In our simulations, the Berendsen thermostats [ReaxFF manual] are applied at two ends of the system. One side of the slab is kept at temperature T_H=300K and the other side of the slab is kept at T_C=150K temperature using these two thermostats. When the system reaches the steady state, a linear temperature profile is established along the ice slab.

The total system is equilibrated at 150K before applying the thermostats. Using the thermostat at the hot side, energy is added to the system and using the thermostat at the cold side of the slab, the energy is withdrawn from the system.

The schematic of the system for calculation of the ice slab TC after deposition on the silica surface is shown in Figure 5. The

hot side thermostat is applied to the lower 500 atoms of silica (T_H=300K) and the cold side thermostat is applied to the top 100 atoms of ice (T_C=150K). The temperatures T_H and T_C of two thin layers of the ice are calculated every 0.25 pico seconds using equipartition theory. Equipartition theory relates the temperature of a system with its average energies.

After the first ice cluster depositions on the silica surfaces, the TC evaluation is performed for the middle 900 atoms inside the ice clusters. These atoms are shown inside a black box in Figure 5.Once steady state is reached, the thermal conductivity, k, is calculated from Fourier's law.

$$K = \frac{< \left|\frac{\Delta E}{\Delta t}\right| >}{A < \left|\frac{dT(z)}{dz}\right| >}$$

The change in energy $< \Delta E >$ is obtained as $< \Delta E > = < \Delta E_H > + < \Delta E_C >$where $< \Delta E_H >$is the time average of kinetic energy change in the hot side and $< \Delta E_C >$ is the time average of the kinetic energy change in the cold side of the system. A is the slab area perpendicular to the heat flux direction and$< |dT(z)/dz| >$ is the time average of the temperature gradient in the direction of the heat flux.

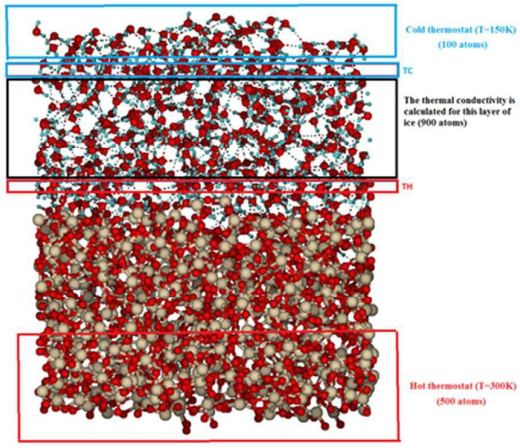

Fig5. Schematic of the system for calculation of the ice TC after ice deposition on the silica surface

Simulation results

Thermal conductivity of amorphous and crystal ice clusters

In order to calculate the TC values for amorphous and crystal ice before deposition on the silica surface, amorphous and crystal ice clusters before deposition on the silica surfaces are studied (Figure3). These values can be compared to the available experimental values for the TC of crystal and amorphous ice to evaluate the accuracy of the method.

Using the dual thermostat method and imposing 200K and 150K temperatures at both ends of the amorphous and crystal ice, the thermal conductivities are calculated. These values along with the available experimental values are mentioned in Table 2, showing that the calculated TC values are in good agreement with the experimental values.

The TC of crystalline ice is larger than that of amorphous ice because the efficient thermal transport in solids arises from lattice vibrations (phonons). In crystalline ice the phonon's mean free path is large enough that it can move over relatively large distances ballistically before being scattered from structural defects. However, for amorphous ice, this effective heat transfer reduces considerably because of the disorder in the structure[58].

Table 2.ReaxFF and experimental values of the thermal conductivity of amorphous and crystal ice

Type of ice	Thermal conductivity from ReaxFF simulations(W/m.K)	Experimental thermal conductivity values (W/m.K)[58, 59]
Amorphous ice	1.4727	1.2-1.4
Crystal ice	2.1788	2.1-2.2

Before studying the TC values for the ice clusters after deposition on the silica surfaces, the TC values of fully oxidized and suboxide silica are calculated by the method similar to the method used for TC calculations of the ice clusters. The TC values are mentioned in Table 3. The experimental value of TC for fully oxidized silica is reported as 1.4 W/m.K[59]. The calculated value of TC for suboxide silica is higher than the TC value for fully oxidized silica. This is contributed to higher Si content in suboxide silica (Table 1). Silicon has a relatively high thermal conductivity value of 149 W/m.K[60].

Table 3.ReaxFF and experimental values of the thermal conductivity of fully oxidized and suboxide silica

Silica type	Thermal conductivity (W/m.K)
Fully oxidized silica	1.8
Suboxide silica	3.47

The phonon mean free path for amorphous ice has been reported to be around 5 Angstrom[61]. Considering the phonon mean free path equation $\lambda \propto k/(\rho C v)$ where k is the thermal conductivity, ρ is the ice density, C is the ice specific heat capacity and v is the sound velocity[62], the mean free path value for crystalline ice should be around two to three times the value of the mean free path for amorphous ice based on the available values for k, ρ and C.

The dimensions of the systems which are studied are at least 27 A which is larger than the mean free path of the ice clusters. Therefore, the method for determination of thermal conductivity values of the ice clusters is reasonable.

For plotting the temperature profile, T(z), as a function of the z coordinate for amorphous ice, after reaching the steady state condition along the ice cluster, four thin slabs are selected at four points along the slab (equal distance in z direction). Each slab includes 100 atoms. The temperature of each slab is calculated based on the equipartition theorem. The calculated temperatures are shown in Figure 6 below. This temperature profile can be estimated as linear profile. Therefore, the Fourier's law is applicable in these simulations.

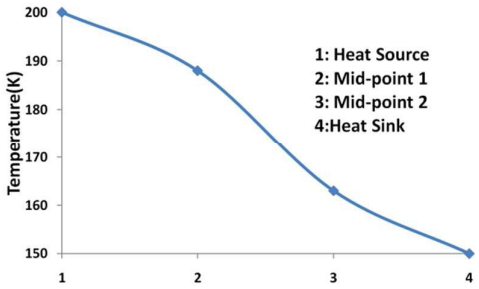

Fig6. Temperature profile, T(z), as a function of the z coordinate for amorphous ice after reaching steady state condition

The TC values for the cases that amorphous and crystal ice deposited on the silica surfaces are shown in Tables 4-7.

Table 4.ReaxFF values of the thermal conductivity of amorphous ice depositing on the fully oxidized silica surface with or without initial impact velocity on the silica surface

Deposition condition	Thermal conductivity (W/m.K)
No impact	0.59
500 m/s impact	0.61
1 km/s impact	0.62

Table 5.ReaxFF values of the thermal conductivity of amorphous ice depositing on the suboxide silica surface with or without initial impact velocity on the silica surface

Deposition condition	Thermal conductivity (W/m.K)
No impact	0.51
500 m/s impact	0.55
1 km/s impact	0.42

Table 6.ReaxFF values of the thermal conductivity of crystal ice depositing on the fully oxidized silica surface with or without initial impact velocity on the silica surface

Deposition condition	Thermal conductivity (W/m.K)
No impact	1.25
500 m/s impact	1.10
1 km/s impact	0.60

Table 7.ReaxFF values of the thermal conductivity of crystal ice depositing on the suboxide silica surface with or without initial impact velocity on the silica surface

Deposition condition	Thermal conductivity (W/m.K)
No impact	1.22
500 m/s impact	1.11
1 km/s impact	0.54

These results show that crystal ice shows higher TC value compared to amorphous ice. Impact of ice on the silica surface causes decrease of TC value for crystal ice compared to the ice deposition without impact. The decrease of the TC value for crystal ice can be attributed to increase of loss in the crystallinity of the structure of first layers of ice after impact (Figure 4). The RDF graphs of the crystal ice before and after 1km/s impact on the fully oxidized silica surface are shown in Figure 7. These graphs are for lower half of the ice cluster that has interface with the silica surface after impact on the silica surface. This loss in the crystallinity is evident in this RDF graph.

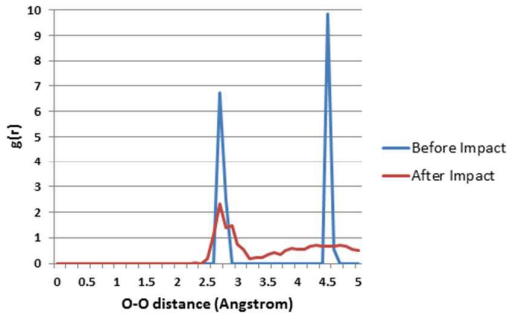

Fig7.RDF graphs of crystal ice cluster before and after 1km/s impact on the surface of fully oxidized silica. These graphs are for the lower half of the ice crystal that has interface with silica surface after impact

The ice clusters on fully oxidized silica shows higher TC compared to the ice on suboxide silica. This is because of a higher degree of irregularity in the ice structure on the suboxide silica. The RDF graphs for the lower half parts of the crystal ice after attaching on the suboxide and fully oxidized silica with impact velocities of 1 km/s are shown in Figure 8. These graphs show that the crystal ice becomes more amorphous in lower layers after impacting on the suboxide silica surface.

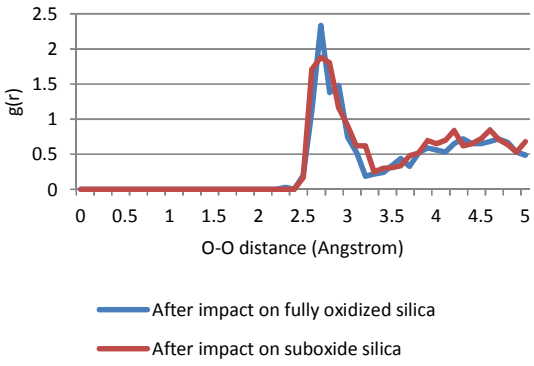

Fig8.RDF graphs of the crystal ice cluster before and after 1km/s impact on the surface of suboxide and fully oxidized silica. These graphs are for lower half of the ice crystal that has interface with silica surface after impact

These results show a drop in the values of TC of the ice clusters after deposition on the silica surfaces compared to the TC values obtained for separate ice clusters. This drop can be attributed to presence of the interface between ice and silica surface and the difference between silica and ice structures. The structural mismatch causes reduction in the heat transfer at the ice-silica interfaces in addition to heat transfer resistance caused by discontinuity.

TC values of crystal and amorphous ice clusters after second impacts on the silica surfaces

In order to investigate the change in the properties of the accreted ice during continued exposure to ice deposition, we investigated the collision of a second ice cluster on the surface of the previously deposited ice. Snapshots of the first and second crystal ice impacts on suboxide silica at 500 m/s and 1 km/s impact velocities are shown in Figures 9 and 10. As shown in these pictures, the retained crystal structure changes at different layers. After deposition of the second crystal ice cluster which impacts on the previously deposited ice with impact velocity of 500 m/s, the crystal structure of the second crystal ice cluster is almost preserved and amorphous structure is not observed in the lower layers of this second ice cluster. Therefore, after the second 500 m/s impact, the crystal ice stays almost intact at top layers. However, the loss of crystal structure is more pronounced at different layers of the second ice clusters impacting at 1 km/s.

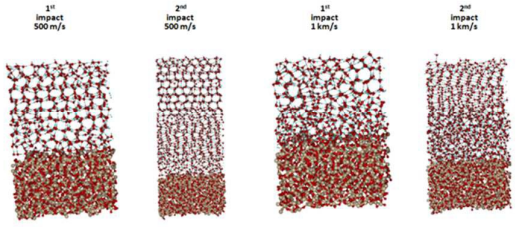

Fig9. First and second impacts of crystal ice on suboxide silica surface at 500 m/s and 1 km/s impact velocities

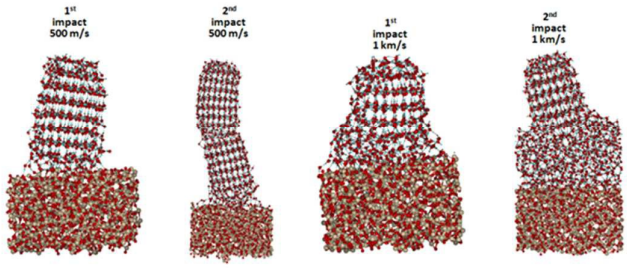

Fig10.Side view of first and second impacts of crystal ice on suboxide silica surface at 500 m/s and 1 km/s impact velocities

In order to calculate the TC values for the deposited ice in these cases, the dual thermostat method is applied to two layers of the ice. Therefore, two values of TC are obtained for each case. Generally the TC values are higher for the top ice layers because there is no silica interface for the top layer and less irregularity is created in the ice structure at the top layers. This can be directly observed in Figures 9 and 10. The RDF graphs of top and bottom layers of crystal ice clusters after the second impact on the suboxide silica surface are shown in Figure 11. This graph shows that the top layer retains the crystal structure better than the lower layer. The TC values are obtained by calculating the TC values at top and bottom layers. These values and the average TC values are mentioned in Tables 8-11. The TC average values are generally higher than the values obtained for the deposited ice clusters after the first impacts because the TC values obtained for the top layers are closer to the TC values for separate ice clusters and therefore, the average will be higher.

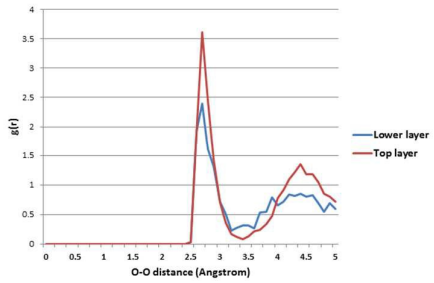

Fig11.RDF graphs of the top and bottom layers of crystal ice cluster after two successive 1km/s impacts on the surface of suboxide silica

Table 8.ReaxFF values of the thermal conductivity of amorphous ice depositing on the fully oxidized silica

Deposition condition	Thermal conductivity (W/m.K)	TC Average value
500 m/s impact($Bottomlayer/Toplayer$)	0.53	0.87
	1.20	
1 km/s impact($Bottomlayer/Toplayer$)	0.54	0.9
	1.25	

Table 9.ReaxFF values of the thermal conductivity of amorphous ice depositing on the suboxide silica

Deposition condition	Thermal conductivity (W/m.K)	TC Average value
500 m/s impact ($Bottomlayer/Toplayer$)	0.57	0.77
	0.96	
1 km/s impact ($Bottomlayer/Toplayer$)	0.54	0.8
	1.05	

Table 10.ReaxFF values of the thermal conductivity of crystal ice depositing on the fully oxidized silica surface

Deposition condition	Thermal conductivity (W/m.K)	TC Average value
500 m/s impact($Bottomlayer/Toplayer$)	1.19	1.44
	1.69	
1 km/s impact($Bottomlayer/Toplayer$)	1.26	1.31
	1.37	

Table 11.ReaxFF values of the thermal conductivity of crystal ice depositing on the suboxide silica surface

Deposition condition	Thermal conductivity (W/m.K)	TC Average value
500 m/s impact($Bottomlayer/Toplayer$)	1.12	1.66
	2.2	
1 km/s impact($Bottomlayer/Toplayer$)	1.07	1.2
	1.33	

Influence of adding ionic 1-Butyl-3-methylimidazolium (BMIM) in the bulk of the amorphous ice cluster on the ice cluster TC value

In many situations, especially at the thruster exit, there are ionic species present in the bulk of the ice clusters. As such, investigating the effect of presence of ionic species in the bulk of ice clusters on the values of the TC is another point of interest in these studies. In order to study the effect of ionic species, we mixed 400 ice molecules with 12 ionic 1-Butyl-3-methylimidazolium (BMIM) molecules and equilibrated the system at 150K (Figure 12). BMIM is an ionic liquid fuel with hypergolic reaction capabilities. These types of ionic liquids can mix with ice clusters at the exit of the thrusters and create ionic ice clusters.

The TC calculations for such mixtures show a drop in the TC values (Table 12). This reduction in TC can be attributed to the more irregularity imposed on the ice structure caused by the presence of the ionic BMIM.

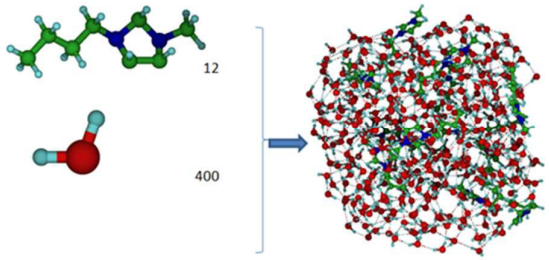

Fig12. Amorphous ice cluster mixed with ionic BMIM

Table 12.ReaxFF values of the thermal conductivity of amorphous ice containing ionic BMIM depositing on the silica surface

Silica type	Thermal conductivity (W/m.K)
Fully oxidized silica	0.53
Suboxide silica	0.32

Conclusions

In this study, the thermal conductivities of ice clusters deposited on silica surfaces are calculated. The ReaxFF reactive force field molecular dynamics simulations of the thermal conductivity (TC) values of crystal and amorphous ice clusters show good agreement with the available experimental TC values. Our results show that the TC value of crystal ice is higher than amorphous ice.

A dual thermostat method is applied to calculate the thermal conductivities. The simulation results show that TC values of the ice clusters decrease after deposition on silica surfaces. Generally, this decrease in TC value is higher in the case of ice deposition on suboxide silica compared to fully oxidized silica surfaces. This is because of the loss of crystallinity in the ice clusters after deposition on suboxide silica surface.

The effect of 500 m/s and 1 km/s impact velocities of the ice clusters on the silica surfaces on the TC values are evaluated. The results show that 500 m/s impact velocity does not reduce

the TC values significantly. But, at 1 km/s impact velocities, the crystal ice lose the crystal structure at its lower layers and this causes a considerable drop in the TC value of the crystal ice cluster deposited on the silica surface after 1 km/s impacts. Studies of the ice clusters after the second impacts show that the top layers of the deposited ice which come from the second ice clusters impacting on the top of the deposited first ice clusters, get less deformed. Therefore, the main contribution in the decrease of the TC values of the ice clusters is from the bottom layers of the deposited ice clusters.

Our calculations also show adding ionic species to the bulk of the ice clusters cause decrease in the value of the TC.

Acknowledgements

This work was sponsored by the U.S. Air Force Office of Scientific Research (AFOSR), Grant No. FA9550-11-1-0158.The views and conclusions contained herein are those of the authors and should not be interpreted as necessarily representing the official policies or endorsements, either expressed or implied, of the AFOSR or the U.S. Government.

References

1 J. Madejski, *International Journal of Heat and Mass Transfer*, 1983, **26**, 1095-1098.
2 M. P. Allen and D. J. Tildesley, *Computer simulation of liquids*, Oxford university press, 1989.
3 Y. Chen, A. Chernatynskiy, D. Brown, P. K. Schelling, E. Artacho and S. R. Phillpot, *Physics of the Earth and Planetary Interiors*, 2012, **210**, 75-89.
4 A. Chernatynskiy, C. Flint, S. B. Sinnott and S. R. Phillpot, *Journal of Materials Science*, 2012, **47**, 7693-7702.
5 A. Chernatynskiy, R. W. Grimes, M. A. Zurbuchen, D. R. Clarke and S. R. Phillpot, *Applied Physics Letters*, 2009, **95**, 161906.
6 A. Chernatynskiy and S. R. Phillpot, *Physical Review B*, 2010, **82**, 134301.
7 A. Chernatynskiy and S. R. Phillpot, *Journal of Applied Physics*, 2013, **114**, 064902.
8 A. Chernatynskiy and S. R. Phillpot, *Current Opinion in Solid State and Materials Science*, 2013, **17**, 1-9.
9 B. Deng, A. Chernatynskiy, M. Khafizov, D. H. Hurley and S. R. Phillpot, *Journal of Applied Physics*, 2014, **115**, 084910.
10 Y. He, I. Savić, D. Donadio and G. Galli, *Physical Chemistry Chemical Physics*, 2012, **14**, 16209-16222.
11 A. Henry and G. Chen, *Physical review letters*, 2008, **101**, 235502.
12 G. Hummer, J. C. Rasaiah and J. P. Noworyta, *Nature*, 2001, **414**, 188-190.
13 S. T. Huxtable, D. G. Cahill, S. Shenogin, L. Xue, R. Ozisik, P. Barone, M. Usrey, M. S. Strano, G. Siddons and M. Shim, *Nature materials*, 2003, **2**, 731-734.
14 M. Khafizov, I. W. Park, A. Chernatynskiy, L. He, J. Lin, J. J. Moore, D. Swank, T. Lillo, S. R. Phillpot and A. El-Azab, *Journal of the American Ceramic Society*, 2014, **97**, 562-569.
15 Y. Liu, H. Yang, N. Liao and P. Yang, *RSC Advances*, 2014, **4**, 54474-54479.
16 J. R. Lukes and H. Zhong, *Journal of Heat Transfer*, 2007, **129**, 705-716.
17 T. Luo and G. Chen, *Physical Chemistry Chemical Physics*, 2013, **15**, 3389-3412.
18 18. E. Lussetti, T. Terao and F. Müller-Plathe, *The Journal of Physical Chemistry B*, 2007, **111**, 11516-11523.
19 B. Ni, T. Watanabe and S. R. Phillpot, *Journal of Physics: Condensed Matter*, 2009, **21**, 084219.
20 M. Nijmeijer, A. Bakker, C. Bruin and J. Sikkenk, *The Journal of chemical physics*, 1988, **89**, 3789-3792.
21 J. W. Pang, A. Chernatynskiy, B. C. Larson, W. J. Buyers, D. L. Abernathy, K. J. McClellan and S. R. Phillpot, *Physical Review B*, 2014, **89**, 115132.
22 E. Rossinsky and F. Müller-Plathe, *The Journal of chemical physics*, 2009, **130**, 134905.
23 P. Shukla, A. Chernatynskiy, J. Nino, S. Sinnott and S. Phillpot, *Journal of Materials Science*, 2011, **46**, 55-62.
24 P. Shukla, T. Watanabe, J. Nino, J. Tulenko and S. Phillpot, *Journal of Nuclear Materials*, 2008, **380**, 1-7.
25 B. Steele, A. Burns, A. Chernatynskiy, R. Grimes and S. Phillpot, *Journal of materials science*, 2010, **45**, 168-176.
26 T. Watanabe, S. B. Sinnott, J. S. Tulenko, R. W. Grimes, P. K. Schelling and S. R. Phillpot, *Journal of Nuclear Materials*, 2008, **375**, 388-396.
27 T. Watanabe, S. G. Srivilliputhur, P. K. Schelling, J. S. Tulenko, S. B. Sinnott and S. R. Phillpot, *Journal of the American Ceramic Society*, 2009, **92**, 850-856.
28 M. Yao, T. Watanabe, P. Schelling, P. Keblinski, D. Cahill and S. Phillpot, *Journal of Applied Physics*, 2008, **104**, 024905.
29 M. Zhang, E. Lussetti, L. E. de Souza and F. Müller-Plathe, *The Journal of Physical Chemistry B*, 2005, **109**, 15060-15067.
30 A. McGaughey and M. Kaviany, *Physical Review B*, 2005, **71**, 184305.
31 A. J. McGaughey and M. Kaviany, *Physical Review B*, 2004, **69**, 094303.
32 J. A. Thomas, R. M. Iutzi and A. J. McGaughey, *Physical Review B*, 2010, **81**, 045413.
33 J. Turney, E. Landry, A. McGaughey and C. Amon, *Physical Review B*, 2009, **79**, 064301.
34 F. Müller-Plathe, *The Journal of chemical physics*, 1997, **106**, 6082-6085.
35 C. Nieto-Draghi and J. B. Avalos, *Molecular Physics*, 2003, **101**, 2303-2307.
36 K. V. Tretiakov and S. Scandolo, *The Journal of chemical physics*, 2004, **120**, 3765-3769.
37 T. Gibbons and S. Estreicher, *Physical review letters*, 2009, **102**, 255502.
38 D. J. Evans, *Physics Letters A*, 1982, **91**, 457-460.
39 G. P. Srivastava, *The physics of phonons*, CRC Press, 1990.
40 J. C. Fogarty, H. M. Aktulga, A. Y. Grama, A. C. Van Duin and S. A. Pandit, *The Journal of chemical physics*, 2010, **132**, 174704.
41 W. G. Hoover, *Computational statistical mechanics*, Elsevier, 2012.
42 A. K. Bharathi, A. Kamat and A. C. van Duin, *Computational and Theoretical Chemistry*, 2012, **987**, 71-76.
43 M. J. Buehler, A. C. van Duin and W. A. Goddard III, *Physical review letters*, 2006, **96**, 095505.
44 K. Chenoweth, A. C. van Duin and W. A. Goddard, *The Journal of Physical Chemistry A*, 2008, **112**, 1040-1053.
45 K. D. Nielson, A. C. van Duin, J. Oxgaard, W.-Q. Deng and W. A. Goddard, *The Journal of Physical Chemistry A*, 2005, **109**, 493-499.
46 J. Ojwang, R. Van Santen, G. J. Kramer, A. C. van Duin and W. A. Goddard III, *The Journal of chemical physics*, 2008, **128**, 164714.
47 A. Rahnamoun and A. van Duin, *The Journal of Physical Chemistry A*, 2014, **118**, 2780-2787.
48 48. A. Strachan, E. M. Kober, A. C. van Duin, J. Oxgaard and W. A. Goddard III, *Thermal decomposition of RDX from reactive molecular dynamics*, DTIC Document, 2005.

49 A. Strachan, A. C. van Duin, D. Chakraborty, S. Dasgupta and W. A. Goddard III, *Physical Review Letters*, 2003, **91**, 098301.
50 A. C. Van Duin, S. Dasgupta, F. Lorant and W. A. Goddard, *The Journal of Physical Chemistry A*, 2001, **105**, 9396-9409.
51 A. C. van Duin, Y. Zeiri, F. Dubnikova, R. Kosloff and W. A. Goddard, *Journal of the American Chemical Society*, 2005, **127**, 11053-11062.
52 D. Raymand, A. C. van Duin, D. Spångberg, W. A. Goddard and K. Hermansson, *Surface Science*, 2010, **604**, 741-752.
53 A. C. van Duin, V. S. Bryantsev, M. S. Diallo, W. A. Goddard, O. Rahaman, D. J. Doren, D. Raymand and K. Hermansson, *The Journal of Physical Chemistry A*, 2010, **114**, 9507-9514.
54 R. M. Abolfath, A. Van Duin and T. Brabec, *The Journal of Physical Chemistry A*, 2011, **115**, 11045-11049.
55 V. V. Hoang, *The Journal of Physical Chemistry B*, 2007, **111**, 12649-12656.
56 Z. Li, A. Borner and D. A. Levin, *The Journal of chemical physics*, 2014, **140**, 224501.
57 Z. Li, A. Borner, A. Ostadhossein, D. A. Levin and A. van Duin.
58 O. Andersson and A. Inaba, *Physical Chemistry Chemical Physics*, 2005, **7**, 1441-1449.
59 W. M. Haynes, *CRC handbook of chemistry and physics*, CRC press, 2014.
60 D. R. Lide, *CRC handbook of chemistry and physics*, CRC press, 2004.
61 J.Klinger, D.Benest, A.Dolfus, R.Smoluchowski, Ices in the solar system, Springer Science & Business Media, 2012.
62 J.M.Ziman, Electrons and phonons : The theory of transport phenomena in solids, Oxford, 2001.